"Wireless Interaction of Neighboring Two Arm Archimedes Spiral Coils in the RF Electromagnet Range"

Anthony J. Kalinowski
Naval Undersea Warfare Center/Div. Npt., Newport, RI 02841-1708

Abstract: The paper addresses a class of problems for modeling and consequently simulating the electromagnetic field radiation pattern from two arms Archimedes spiral coils. The frequency spatial wavelengths relative to the coil dimensions are in a range where the electromagnetic Maxwell's equations are solved numerically via the RF module. The application considered has multiple flat double spiral coils, separated by standoff distance L, that are embedded at the interface between two dielectric materials (i.e. the coil spiral is in a plane parallel to the interface layer). Each layer (referred to as Outer and Inner) has it's own relative permittivity ε^o_r and ε^i_r , and the upper layer is also bounded above by an infinite lossy domain of permittivity ε^I_r . The response quantity of particular interest is knowledge of the radiated magnetic field **H** and electric field **E** both in the neighborhood of the drive coil and in neighboring receive coils without direct wire connections between them. Also of interest is the ratio of the induced (wireless) receive coil current –to- the drive coil current $|(I_R/I_D)|$ as measured through the coil's lumped input-output port stations.

The base legs of the two arms of the coil are driven independently by voltages V_1 and V_2 and corresponding phases of ϕ_1 and ϕ_2 , via impedance lumped ports of the type available in COMSOL. The radiation pattern can be steered in a plane parallel to the upper and lower layer interface by changing the ratio of V_1/V_2 and/or phase of V_1 relative to V_2. Further it is shown that the radiation can be confined in the lower layer by appropriately adjusting the permittivity ratio $\varepsilon^o_r / \varepsilon^i_r$ between the outer and inner layers.
.

Keywords: Electromagnetic Radiation, FEM modeling of coils.

1. Introduction

The application of interest herein, is to radiate strong magnetic fields in a two-layered dielectric medium, bounded by a third infinite medium from above. Of particular interest, is the situation where most of the electromagnetic radiated field is kept within the inner layer. Voltage driven flat coils have been selected as the radiator, because they nicely lie along the interface between the two dielectrics (typically solid materials). The paper treats the problem of solving for the driven radiated electric **E** field and magnetic **H** field emanating from a two arm Archimedes spiral coil as illustrated by the model shown in Fig. 1. This type coil has been used as an antenna as discussed for example, in Ref.[1]. The polar form of the radius R of the first arm of the coil centerline is variable and unfolds according to the relation

$$R(\theta)=R_o+R_o\,\theta \qquad \text{Eq (1)}$$

where θ is the cylindrical coordinate angle, and R_o is an off set constant starting radius at $\theta = 0$. A second arm can be created by rotating a copy of the first arm by 180^o .

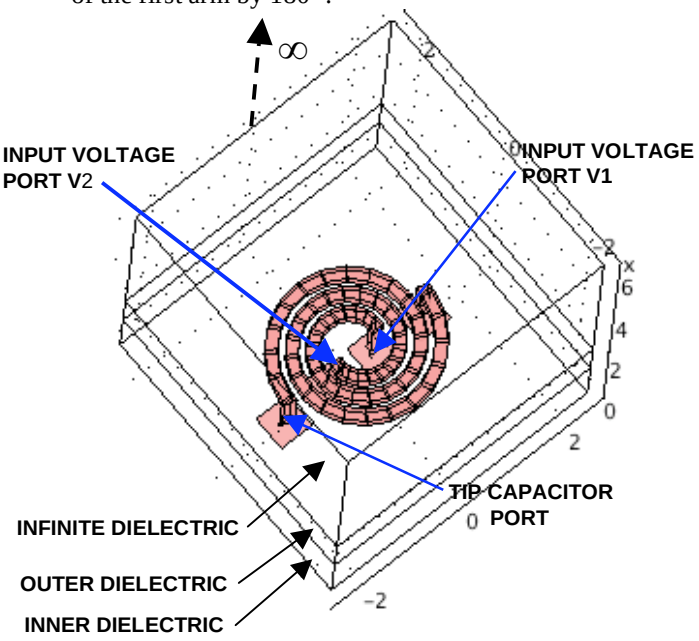

Figure 1. Isolated 2-Arm Archimedes Spiral Coil Model

The response of a single type of coil was considered in a closely related paper Ref.[5], where sensitivities to (a) the effect of feed line input port impedance Z_p (b) effect of inner dielectric permittivity ratio, $\varepsilon^i_r / \varepsilon^o_r$, for the

problem type shown in Fig. 1, (c) effect of coil geometry (circular spiral vs. elliptical spiral), and (d) variation of arm 1 feed voltage (V1) magnitude and phase vs. arm 2 feed voltage (V2) magnitude and phase, while holding total feed voltage |V1|+|V2|=constant. This follow on paper will pass through a sequence of increasingly complex problems, where the wireless transfer of power from one sender coil to a row of remotely placed receiver coils is treated. Here we take advantage of what was learned earlier and apply it towards evaluating the wireless transfer of power (i.e. the ratio of the induced receive coil current –to- the drive coil current $|(I_R/I_D)|$) for the situations:

a) One coil free field vs. row of 5 receivers
b) Shape effect: Circular vs. ellipse coils
c) Sensitivity of dielectric permittivity ratio $\varepsilon^i_r / \varepsilon^o_r$
d) Steering radiation beam with port phasing
e) Two rows of receive coils and interference of front row on back row
f) Sensitivity of receive coil separation distance ratio L/D_c .

1.1 Past Works

The response to spiral coils of the type considered herein (e.g. Fig. 1), is a complicated 3D field that is well beyond closed form analytical solutions. There are two competing numerical methodologies for solving Maxwell's equation in the RF domain, where the physical size of the electromagnetic components (e.g. coils, and capacitors) are on the order of the electromagnetic medium wave length λ:

$$\lambda = c_o / (f\sqrt{\mu_r \varepsilon_r}) \qquad \text{Eq(2)}$$

where c_o is the speed of light in vacuum, f is the wave frequency, ε_r is the relative permittivity, and μ_r is the relative permeability. The two candidate techniques are the finite element method (FEM) Ref.[2] and the finite difference method (FDM) Ref.[3]. The FEM has the advantage that it is more readily applied to situations where the configuration has irregular shaped obstacles, and therefore COMSOL was selected as the computational program for solving the problem at hand.

2. Governing Equations

The governing equations for the total electric field **E** in the dielectric domain (for time harmonic type response) are given by Maxwell's equations:

$$\nabla \times (\mu_r^{-1} \nabla \times \mathbf{E}) - k_0^2 (\varepsilon_r - \frac{i\sigma}{\omega \varepsilon_0})\mathbf{E} = \mathbf{0} \quad \text{Eq(3)}$$

and are solved for **E** using the RF module in COMSOL.

2.1 Surface Boundary Conditions

The mesh termination at top and side boundaries of the FEM model shown in Fig. 1 must include some sort of radiation absorbing boundary condition. Two types were considered, namely the PML (perfectly matched layer), and COMSOL's built in scattering boundary condition (used herein), namely: $nx(\nabla xE) - iknx(Exn) = 0$. For interfaces between two unlike materials, such as between the outer and inner dielectric as shown in Fig. 1, the continuity boundary condition of $nx(E_{out} - E_{in}) = 0$ is used. The floor of the model is terminated with a PEC boundary condition (perfect electric conductor).

The copper wire that makes up the coil is not modeled directly in the usual finite element sense (i.e. with a distribution of 3-D solid elements all the way through the thickness of the coil). The surface currents are limited to a very thin region ("skin effect as described in Ref.[2]), so instead, the copper coil is modeled with an equivalent surface impedance boundary condition applied only to the surface of the wire. The coil wire is therefore modeled as a "*wormhole*" passing through the dielectric medial, where the copper surface impedance boundary condition is applied at these wormhole surface elements, and is implemented as standard boundary condition offered within the COMSOL menu list of applicable boundary conditions.

Finally, the input voltage needs to be applied into the base of the coil (labeled as *input voltage port V1* and *input voltage port V2* in Fig. 1). Relatively new to the RF module, is the ability to avoid complex modeling of an actual input wire with some Z impedance rating, which is replaced with a COMSOL "*lumped port*" boundary condition. This amounts to modeling a planar rectangular tab that connects from the end of the coil –to- some sort of grounding plane (e.g. one the four square appearing feet at the base of the Fig. 1 model). Note there are two feet for the drive ports and two for the capacitor-loaded tips.

The square feet of these grounding planes are also modeled with a copper surface impedance boundary condition like the wormhole surface.

2.2 Lumped Port Boundary Conditions

Here we address the parameter assignments applied to the lumped ports. This is where three items are assigned:

i) the voltage input feed (optional), $V = V_o e^{i\phi\pi/180}$, where V_o is the voltage input and ϕ is the phase angle in degrees.

ii) port type (uniform selected here)

iii) Lumped port impedance Z_{ref} (real for resistance and imaginary for capacitance)

2.3 Mesh sizing

For harmonic steady state problems, the mesh size is set according to the shortest wavelength expected during the event. For example, if N_{ew} is the number of elements/wave length required for accurate modeling and C_{min} is the slowest wave speed, and f_{max} the largest frequency experienced in a frequency sweep, then the mesh can be sized with $\Delta_{min} = C_{min} / (N_{ew} f_{max})$, (e.g. N_{ew} =6 for quadratic element shape functions). We note that the building blocks showing the 3-D coil in Fig. 1 (or later in Fig. 3a) are not the finite elements, but rather the geometry building blocks that construct the coil (i.e. the actual surface mesh is finer than the blocks).

3. Applications

Next we give examples of the six problem types (a,b,c,d,e,f) outlined in the introduction section.

3.1 General Model Description

Here we define the basic model configuration before any variations in parameters are introduced. The overall model domain size is small (.05 cm x .05 cm x .062 cm), however the frequencies are high ($O(10^{11})$), where the RF wavelengths are on the order of the coil diameter of D=.027 cm . Our interest herein is mainly on the relative **H** field shapes (i.e. relative based on variation of the parameters specified in the problem types {a,b,c,d,e,f} and on the spatial range of the radiation **H** and **E** fields). The same shape sensitivities scale upward to larger dimensions, but with lower frequencies (assuming the electromagnetic material constants do not appreciably change with frequency). For example, in the models shown later, if S=100 is the dimension scale factor, multiplying all dimensions by S and multiplying the frequency by 1/S produced essentially the same shape radiation fields.

Geometry parameters flat circular spiral coil

The centerline of the coil is given by Eq(1) with the offset parameter R_o = .01 cm with a coil thickness of 0.02 cm. However with this thickness coil, the coil is too thick near the origin where external coil surfaces across from each other can overlap. Therefore the starting angle in the coil spiral is set at $\theta_s=\pi$, where θ is swept out for $\theta_s \le \theta \le \theta_s + 3\pi$. The R($\theta$) sweep for the circular spiral centerline is shown later in Fig. 3b. With this non zero θ_s , the starting spiral radius becomes $(1+ \pi)$ R_o , and surface overlap problems are eliminated .

Location of flat spiral coil

The location of the flat coil is positioned between the two dielectrics, with the coil thickness located within the inner dielectric. Later results showing side views (e.g. Fig. 2a) illustrate the depth location more clearly.

Material parameters:

The following material parameters were used for as the ***base case*** *starting parameters* of interest to this work:

Relative to the Fig. 1 model:

Outer Diel. $\varepsilon^o_r = \varepsilon_B$;

Inner Diel. $\varepsilon^i_r = .75\varepsilon_B$;

thus $\varepsilon^i_r / \varepsilon^o_r = .75$

Cu Coil $\varepsilon^c_r=1.0$; $\mu^c_r= 1.0$; $\sigma^c_r= 6.0e7$[S/m]

Infinite Diel. $\varepsilon^I_r / \varepsilon^o_r \approx 4$; $\mu^I_r= 1.0$; $\sigma^I_r=7.0e\text{-}6$[S/m]

Coil Voltage Arm Loading

The *base case* coil lumped port loading was for unit voltage and zero phase:

$V_1=1.0$ $\phi_1=0$ deg. and $V_2=1.0$ $\phi_2=0$ deg. where this is the loading used in all example unless otherwise stated

Lumped Port Impedances

Arm Drive ports 1 and 2 Zp=50 Ω

Arm Tip Ports 3 and 4 Zp=-iω/C

where C=tip capacitor input.

Solver Method

Three-dimensional problems rapidly become unmanageable unless measures are taken to deal with large degree of freedom models. Most of the models are run with 4 -to- 9.5 million

unknowns on a 4-processor 64G core memory 64bit based Windows^{XP} operating system. Direct solvers run out of memory for our size problems, and therefore advantage of memory friendly iterative solver (GMRES) are employed, using a *geometric multigrid preconditioner* (right handed), a *SOR vector presmoother*, a *SORU vector postsmoother* and a *SPOOLS coarse solver*. These worked fine as long as the mesh had a reasonable number of elements/wavelength distribution. For example 7 million unknowns often reach convergence in approximately 180 min. per frequency.

Field Response Recording

The tangential component of the magnetic field, Ht, in the X-Y plane of the spiral flat coil is the electromagnetic field quantity selected for display. The **H** field tends to propagate out radial from the center of the coil, where the strongest component of the **H** vector is tangent to the cylindrical coordinate r direction centered at the coil center, namely H_t. The field variables computed are the Cartesian components of **H,** so the XY plane H_t component is post-processed according to

$$H_t = \frac{yH_x}{\sqrt{x^2+y^2}} - \frac{xH_y}{\sqrt{x^2+y^2}} \qquad \textbf{Eq(4)}$$

where the H_x and H_y coefficients are simply sin and cos rotation quantities. In all the field plots shown later, all X-Y plane planar contour plots are in the inner dielectric, at a z=constant sliced plane located at the bottom thickness of the spiral coil. The dominant response is outward propagating curved wave fronts from the coil center, where like the $\mathbf{H_t}$ EM wave planar fronts, the E_z component of the electric field **E** (which is $\perp$ to H_t) is similar in shape to H_t (but not shown herein).

Coil Current Recording

The current going into the lumped ports on the drive coil and the output current harvested on the receive coils can be directly evaluated in the post processing section under Post processing -> Data Display->Global by evaluating the built in COMSOL variable Iport_i_gj_rfw, where **i** is the port number and **j** is the 3D geometry label in Geom**j** that were previously assigned at the model building stage.

Efficiency Evaluation

In all subsequent discussions, it is of interest to compute the net harvested wireless induced current in the downstream receive coils. We define the net current harvested by N_c receivers as

$$I_{eff} \equiv |I_R|/|I_D| = \sum_{n=1}^{n=Nc} |I_n|/|I_{IN}| \qquad \textbf{Eq(5)}$$

where for example in most cases herein (except where otherwise stated), Nc=5 and I_{IN} is the current fed into both of the send spiral input ports in Fig. 1 .

3.1.1 Basic Circular Spiral Model

In a related work, Ref.[5], it was discovered that in order to achieve stronger radiated fields in the plane near the interface between the two dielectrics, the inner to outer permittivity ratio had to be changed beyond the base case described in section 3.1, namely increase the inner to outer dielectric ratio ε^i_r / ε^o_r from the base case value of .75 to 1.5 . The 1.5 ratio was achieved by simply doubling the inner dielectric base case $\varepsilon^i_r = 2x\varepsilon_B$, so we begin with doubling.

Based on frequency sweeps done on the new model with the infinite domain above the outer layer, it was found that the best range with the strongest H_t fields was for $5.5e11 \leq f \leq 6.0e11$ which was roughly the same as the earlier work of Ref.[5], even though here we have a different top-of-model boundary, (i.e. ε^I_r infinite domain).

The model solved for first, will be a benchmark case that also will be used later for subsequent comparisons to different variations on this basic model. We start with a free field model (driver only) followed by the same case, except this time with 5 down stream coils where each receiver coil is just like the drive coil. The driver coil in both cases is loaded without phasing, so V_1=1.0 ϕ_1=0 deg. and V_2=1.0 ϕ_2=0 deg. and drive to receive coil separation L/D_C=9.25.

Free Field (driver only)

The free field is shown in Fig. 2a, where the Mag(H_t) is shown plotted in an XY plane plan view, at a cut (z=constant), corresponding to a cutting plane level just below the coil thickness (for example view the fine red dashed line in the side view ZY plane cut of Fig. 2a). The ZY plane side view slice is made down the middle at cut x=0, where the origin coordinate system in the model and in all subsequent models is shown at

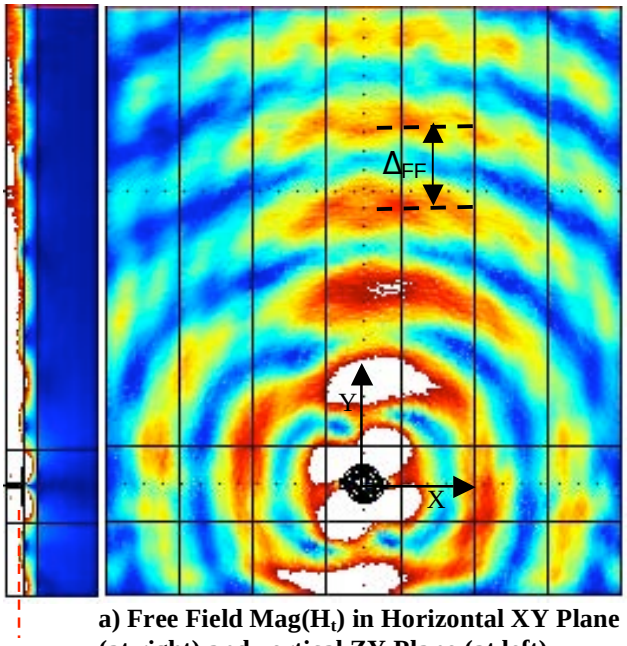

a) Free Field Mag(H_t) in Horizontal XY Plane (at right) and vertical ZY Plane (at left)

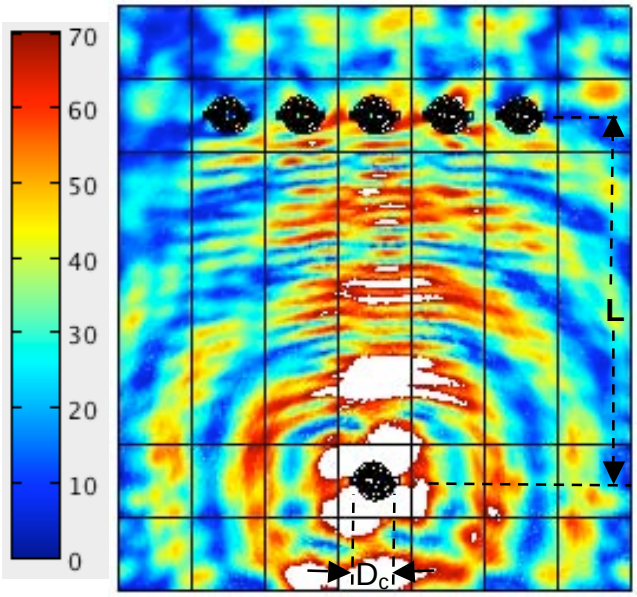

b) 5 Receivers: Mag(H_t) in Horizontal XY Plane, where efficiency $|(I_R/I_D)|$ = 63.7%

Figure 2. Mag(H_t) for Free Field vs. Row of 5 Receivers, for Double Base Case $\varepsilon^i_r / \varepsilon^o_r$ = 1.5 at f=6 e11Hz., L/D_C=9.25

the center of the drive coil as indicated in Fig. 2a (right view). Any white zones shown are beyond the max range of the contour cutoffs. The result shows that the "hottest" part of the magnetic **H** field lies confined within the inner layer. It is noted that in this plot and others to follow, the scale is such that the coil detail is blurry, however the actual block containing a clear view of the coil is shown in Fig. 1.

<u>One Row of 5 Receivers</u>

The corresponding XY plot in Fig. 2b shows the same driven model, but now in the presence of 5 receiver coils. There are some reflections from the receive coils, which slightly alters the details of the $\mathbf{H}_t$ field, however the overall structure of the field is similar. The net current harvested, using Eq(5) with N_c = 5, is 63.7%, at a coil send-to-receive separation of L/D_c=9.25.

3.2 Effect of Coil Geometry (Circular Spiral vs. Elliptical Spiral) on Efficiency Ratio $|(I_R/I_D)|$

Next we consider the effect of the coil cross sectional shape on the radiated magnetic field. The motivation here is the potential of having some unusual radiation effects, such as having a stronger focused beam in the Y direction. The equation for the spiral centerline, given by Eq(1), is modified by replacing the R_o with R'_o

$$R(\theta) = R'_o + R'_o\,\theta \qquad \text{Eq (6)}$$

where:

$$R'_o = \sqrt{\frac{(\alpha R_o)^2}{1-\cos(\theta)^2(1-\alpha^2)}}$$

with α=(semi-minor axis) / (semi-major axis) of base ellipse, and R_o is the same value used in the circular Eq(1). The R'_o formula, is the polar form of an ellipse for radius vs. θ. As in the circle spiral, we use the same offset parameter R_o=.01 cm with a coil thickness of 0.02 cm, α=.75 and a starting angle in the coil spiral of $\theta_s=\pi$, where θ is swept out for $\theta_s \le \theta \le \theta_s + 3\pi$. We note that Eq(6) reduces to Eq(1) when $\alpha \to 1.0$. The resulting spiral ellipse centerline vs. spiral circular centerline comparison is shown in Fig. 3b and the corresponding finite element geometrical block segments filled out about the centerline (before filling with finite elements) is shown in Fig. 3a.

<u>One Row of 5 Receivers</u>

The corresponding XY plot in Fig. 4 corresponds to the same model and conditions used in Fig. 3b, but now in the presence of 5 elliptical shaped driver and receiver coils. Upon observing Fig. 4

it is evident that the ellipse shaped coil is a narrower beam, however the net current harvested over all 5 receivers, using Eq(5) with N_C = 5 is 64.6% which is only slightly better than the 63.7% for the circular coils. The distribution of current generation over the coils is different however, as illustrated in Table 1.

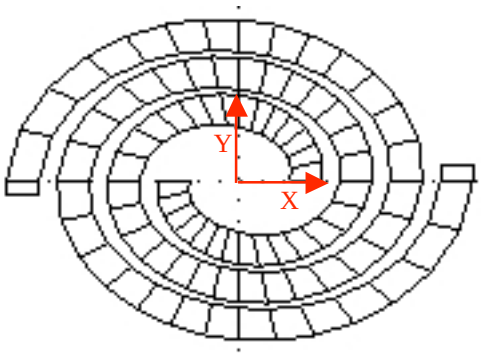

a) XY View of Ellipse Spiral Coil Shape α=.75

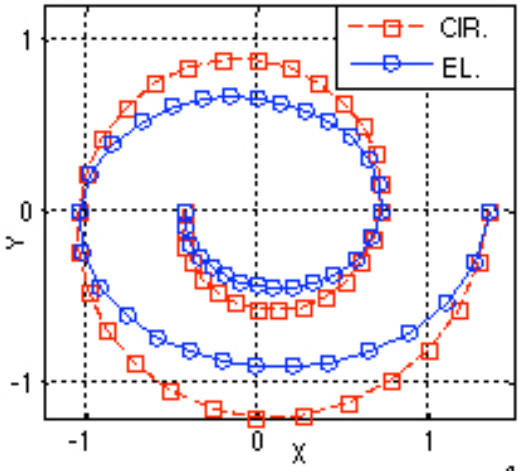

b) Circle (α=1.0) vs. Ellipse (α=.75) Spiral Centerline

Figure 3. Ellipse Coil Cross Section

Upon processing the data over a sequence of: N_c=5 (i.e. all receive coils), then N_c=3 (i.e. middle 3 receive coils) and finally N_c=1 (i.e. middle 1 receive coil), it is observed that most of the recovery is coming out of the middle 3 coils, with the center one being the strongest recovery.

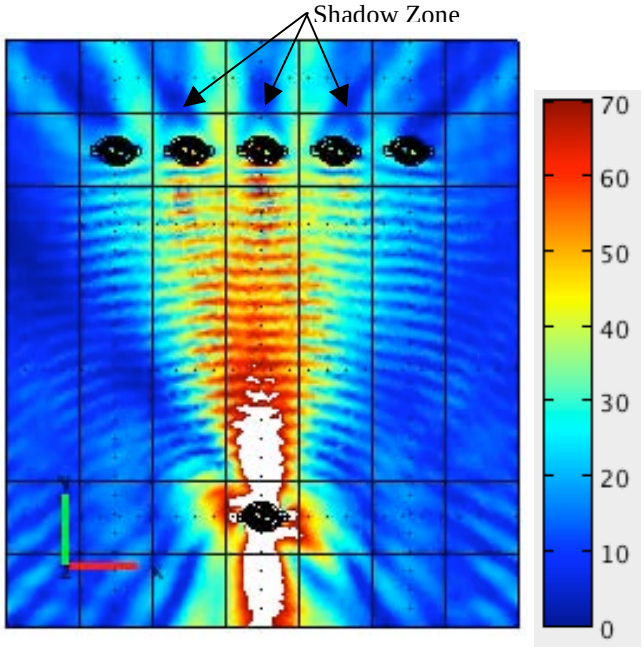

Figure 4. Mag(H_t) for Row of 5 Elliptical Receivers and 1 Sender, for Double Base Case $\varepsilon^i_r / \varepsilon^o_r$ = 1.5 at f=6e11 Hz where efficiency $|(I_R/I_D)|$ = 64.6%

Table 1. Efficiency Distribution Over Receive Coils for $\varepsilon^i_r / \varepsilon^o_r$ = 1.5 at f=6e11 Hz

Shape / I_{eff}	I_{eff} @N_c=5	I_{eff} @N_c=3	I_{eff} @N_c=1
Elliptical	**64.6 %**	**51.5%**	**31.0%**
Circular	**63.7 %**	**38.8%**	**18.4%**

Finally, it is of interest to note that there are shadow zones directly behind the receive coils. Therefore any other coils directly placed behind these front 5 might have a problem being excited as strongly as the front 5. This interference point will be further explored later in the section 3.5 for two rows of circular coils.

3.3 Sensitivity of inner to outer dielectric permittivity ratio ε^i_r / ε^o_r on Efficiency Ratio $|(I_R/I_D)|$

The earlier related Ref[5] work showed that increasing the inner to outer dielectric ratio ε^i_r / ε^o_r from the base case value of 0.75 to 1.5 improved the radiation patterns. However, seeking out material changes that would achieve this increase beyond the existing base case materials might prove to be difficult. Therefore here we back off on the 2.0xBase Case and

instead invoke a less drastic change, namely for 5/4xBase Case, so we select $\varepsilon^i_r/\varepsilon^o_r = 15/16$ .The different material constant changes the frequency band where the system best performs, thus for this new case, good performance is achieved for 7.0e11≤ f ≤ 7.5e11 Hz . The solution shown in Fig. 5 then, is the same as the Fig. 2b case, except here f=7.0e11 Hz (rather than f=6.0e11 Hz), and $\varepsilon^i_r/\varepsilon^o_r = 15/16$ (rather than $\varepsilon^i_r/\varepsilon^o_r = 1.5$).

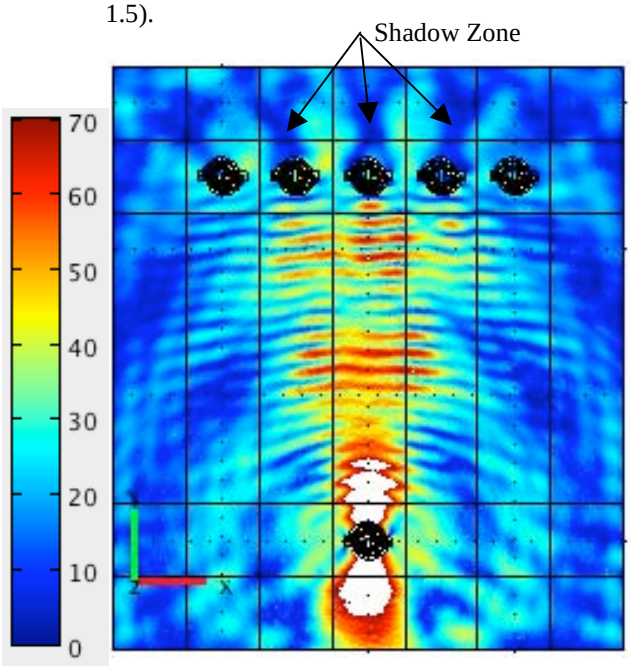

Figure 5. Mag(H_t) for Row of 5 Circular Receivers and 1 Sender, for 5/4xBase Case $\varepsilon^i_r/\varepsilon^o_r = 15/16$ at f=7e11 Hz where efficiency $|(I_R/I_D)| = 50.8\%$.

The resulting efficiency decreased from $|(I_R/I_D)|$ =63.7% to the new value of $|(I_R/I_D)|$ =50.8% as a price for using the smaller permittivity ratio.

3.4 Steering Radiation Beam Using Port Phasing With Receive Elements Along the Side

The previous examples have the orientation of the drive and receive coils in similar positions (e.g. the feet at the base of feed coils arms are in line horizontally, i.e. parallel to the X axis). The receive coils were in a row parallel to the X-axis in all earlier examples; however, here the drive coil stays in the same orientation, but the

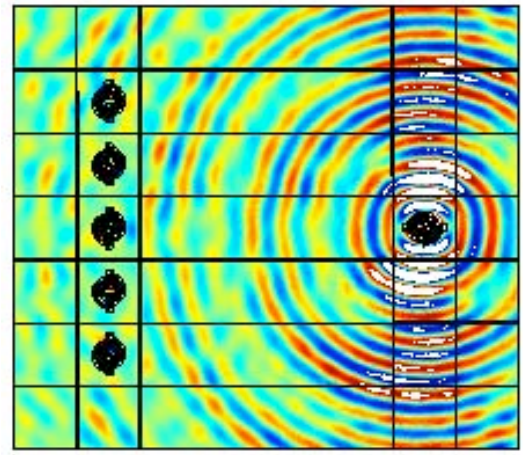

a) Without Phasing 5 Receive Coils: Real Part(H_t) in Horizontal XY Plane, V_1=1.0 ϕ_1=0° and V_2=1.0 ϕ_2=0° where efficiency $|(I_R/I_D)|$ = 31.0%

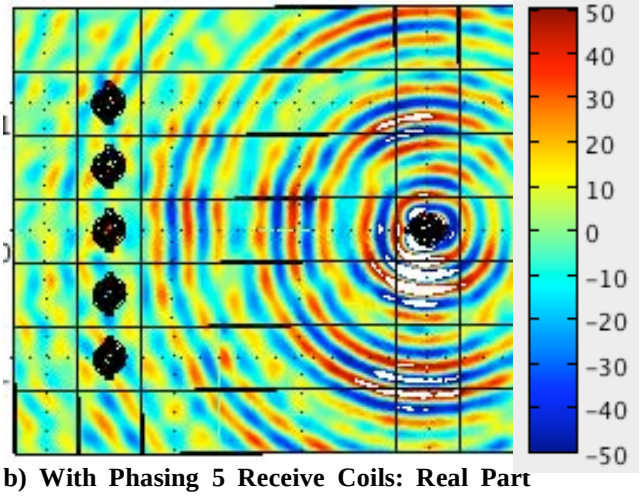

b) With Phasing 5 Receive Coils: Real Part (H_t) in Horizontal XY Plane, V_1=1.0 ϕ_1=0° and V_2=1.0 ϕ_2=-90 where efficiency $|(I_R/I_D)|$ = 46.3%

Figure 6. Phase Steer: Real Part(H_t) for Row of 5 Circular Receivers and 1 Sender, for 5/4 x Base Case, $\varepsilon^i_r/\varepsilon^o_r = 15/16$ at f=7.5e11 Hz

receive coils are rotated 90° and orientated along the side in a line parallel to the Y-axis. This example also illustrates how the phase of the input drive ports can be changed in a manner to favorably modify the radiation pattern and (I_R/I_D). The result in Fig. 6a shows the resulting $\mathbf{H_t}$ field for the no phasing case with parameters $\varepsilon^i_r/\varepsilon^o_r$ = 15/16, f=7.5e11 Hz, and no phasing drive data V_1=1.0 ϕ_1=0° and V_2=1.0 ϕ_2=0°, resulting in an

efficiency ratio of $|(I_R/I_D)|$ = 31.0% with (N_c=5) . In this example (and the next 3.5 section), the real part of the complex magnetic H_t field is plotted instead of the magnitude, so that the sign change of the $\mathbf{H_t}$ roll off with increasing radial component from the coil center, illustrates a traveling wave like structure of the magnetic field. The white zones of this plot indicate that the plotted quantity is beyond the outer extremes of the color legend (e.g. as one might expect the strongest part of the field is closest to the coil and therefore appears white).

The result in Fig. 6b, is the same as Fig. 6a except the phase of the second leg is phased 90° V_1=1.0 ϕ_1=0° and V_2=1.0 ϕ_2=-90° where efficiency is increased to $|(I_R/I_D)|$ = 46.3% .

3.5 Two Nonsymmetrical Receive Rows and Interference of Front Row on Back Row

This example treats the case where: (a) the receive coils are not symmetrically placed and (b) there is the presence of a second row of coils behind the first and therefore the issue of interference comes into play. The model is like the one in section 3.3 except here the receivers are placed non-symmetrically and the drive legs are phased to send more field strength to the right. The model parameters are for the 5/4xBase Case, $\varepsilon^i_r / \varepsilon^o_r$ = 15/16 at f=7e11 Hz, and the drive legs are phased according to V_1=1.0 ϕ_1=0° and V_2=1.0 ϕ_2=+90°. The sign on the phasing to steer left vs. right was established in Ref [5].

<u>One Row of 5 Receivers</u>

The efficiency ratio here, for N_c=5, is $|(I_R/I_D)|$ = 42.9% as shown in Fig. 7a and is a reduction as compared to the symmetric case in, Fig. 5 of $|(I_R/I_D)|$ = 50.8%. The reduction is most likely due to the fact that the H_t field is weaker for the end coils in the nonsymmetrical row.

<u>Two Rows of 5 Receivers</u>

Here we add an additional row of 5 in front of the original row of 5 already in place as used in the previous Fig. 7a case. The efficiency ratio here for, N_c=10, is $|(I_R/I_D)|$ = 76.6% as shown in Fig. 7b and is not quite double (i.e. 85.8% would be double) the current harvested in the corresponding 5 row case of Fig. 7a. The reason is due to the interference of the front coils on the corresponding back coils (e.g. shadow zones that can appear behind lead coils as in related Fig. 5).

Comparing the H_t field in the side view of the 5

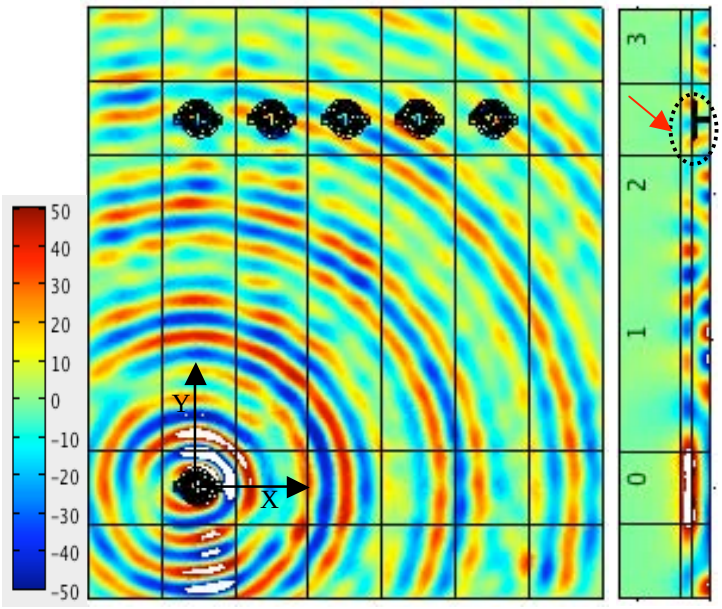

a) 5 Receive Coils: RealPart(H_t) XY Plane and side YZ plane, V_1=1.0 ϕ_1=0° and V_2=1.0 ϕ_2=+90° where efficiency $|(I_R/I_D)|$ = 42.9%

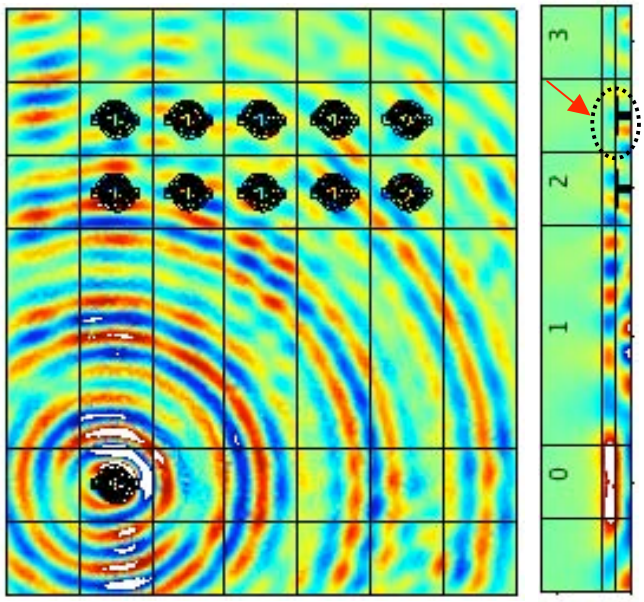

b) 10 Receive Coils: RealPart(H_t) in XY Plane and side YZ plane, V_1=1.0 ϕ_1=0° and V_2=1.0 ϕ_2=+90° : efficiency $|(I_R/I_D)|$ = 76.6%

Figure 7. Real Part(H_t) for Row of 5 VS. Row of 10 Circular Receivers and 1 Sender, for 5/4 x Base Case $\varepsilon^i_r / \varepsilon^o_r$ = 15/16 at f=7e11 Hz

row alone case in Fig. 7a (dashed oval with arrow marker) to the same field zone with the additional row in front as shown in side view of Fig. 7b, we see that the field is weaker on the back coil when the front coil is in place. These YZ side view cuts are at X=0, thus slicing through the drive coil and left most receive coil.

3.6 Sensitivity of Efficiency to Receive Coil Separation Distance Ratio L/D_c

This example addresses the sensitivity of the efficiency ratio on the separation distance between the drive and receive coils, which we define with the variable L/D_c , where L and D_c are shown in Fig. 2b. We start with the basic benchmark model of Fig. 2b, having parameters 2xBase Case $\varepsilon^i_r / \varepsilon^o_r = 1.5$ at f=6e11 Hz, and the drive legs are loaded according to V_1=1.0 ϕ_1=0° and V_2=1.0 ϕ_2=0°. Next the separation parameter is swept out in equal intervals over the

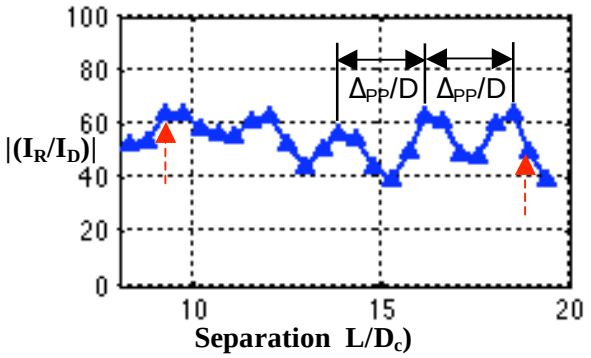

Figure 8. Efficiency $|(I_R/I_D)$ %| for Row of 5 Circular Receivers vs. Separation (i.e. L/D_c), for Double Base Case $\varepsilon^i_r / \varepsilon^o_r = 1.5$ at f=6e11 Hz

range $8.33 \le L/D_c \le 19.4$ where the efficiency sweep of $|(I_R/I_D)|$ is shown in Fig. 8. Two field plots are selected for display, firstly the already shown benchmark case in Fig. 2b where the separation was L/D_c =9.25 with efficiency $|(I_R/I_D)|$ = 63.7% and secondly here in Fig. 9 where the efficiency, at L/D_c =19.0, falls off to $|(I_R/I_D)|$ = 49.3% . The Fig. 8 dashed arrow markers correspond to these specific Fig. 2b and Fig. 9 field plots. We note in Fig. 8 that the efficiency fluctuates with L/D_c over the plot range. We speculate that this is due to where the receive coil is positioned in relation to the highs or lows in the $Mag(H_t)$ in the corresponding free field. For example the peak-to-peak spacing Δ_{FF} of the free field **$Mag(H_t)$** maximums in the y direction of Fig. 2a, normalized to the coil diameter D_c , is $\Delta_{FF} / D_c \approx 2.1$ and this value is on the order of the peak-to-peak spacing of the efficiency fluctuations $\Delta_{PP} / D_c \approx 2.3$ as marked in the Fig. 8 plot.

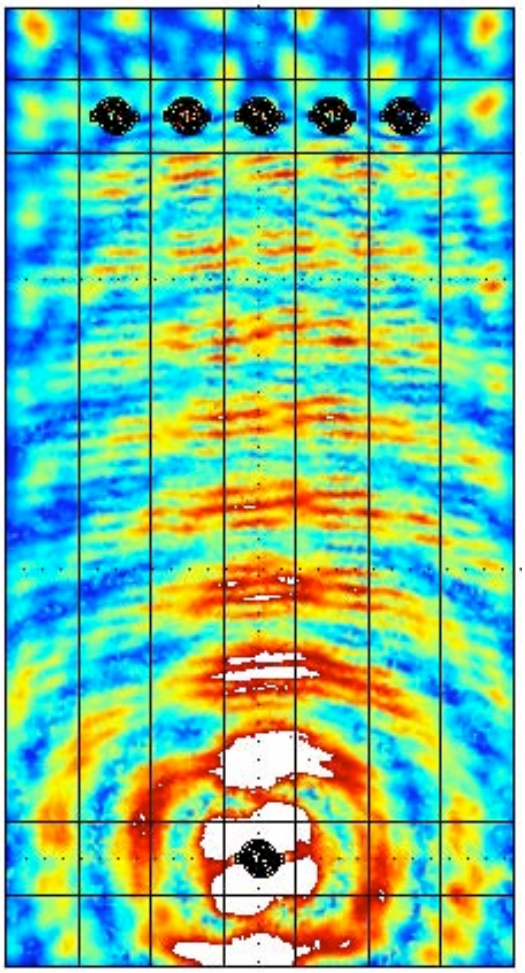

Figure 9. $Mag(H_t)$ for Row of 5 Circular Receivers at Long Separation (i.e. L/D_c =19.0), for Double Base Case $\varepsilon^i_r / \varepsilon^o_r = 1.5$ at f=6e11 Hz with efficiency $|(I_R/I_D)|$ = 49.3%

4. Conclusions

The results in this paper illustrate how COMSOL is used to solve for the radiated electromagnetic fields in the 3-D space surrounding the flat spiral send and receive coils and for the corresponding wirelessly transmitted harvested current, in a RF

frequency range where the dimensions of the coil are on the order of an electromagnetic wavelength. The results show that by altering the shape of the spiral coils (circular vs. elliptical), current harvesting is more focused and also by varying the phase of the two arm coil feed lines, it is possible to distort the shape and direction of the radiated field, such as pointing the radiation away from a particular direction, such as in Fig. 6 where the efficiency ratio $|(I_R/I_D)|$ is improved from 31% to 46.3% . Also, we showed by appropriately adjusting the permittivity ε^i_r / ε^o_r ratio of the inner-to-outer dielectric layers, and adding a unbounded infinite domain above the outer most layer with relative permittivity ε^l_r / $\varepsilon^o_r \approx 4.0$, most of the radiation was confined to the inner layer along the path from the drive to receive coil. Finally, the efficiency ratio $|(I_R/I_D)|$ vs. normalized separation distance L/D_{coil} , showed a good performance over a large range of separation distances where the fluctuations in efficiency vs. distance were correlated to similar fluctuations in the free field $Mag(H_t)$ values of a single send coil.

References

1. Johnson, Richard C., Antenna Engineering Handbook, Third Edition, McGraw Hill, Inc., NY, 1993.

2. Jim Jianming, The Finite Element Method in Electromagnetics, Second Edition, John Wiley and Sons, 2002

3. NguTaflove Allen and Susan C. Hagness Susan (2005), *Computational Electrodynamics: The Finite-Difference Time-Domain Method, 3rd ed.*. Artech House Publishers.

4. COMSOL Inc. (www.comsol.com)

5. Anthony J. Kalinowski and Jason Maguire (2008), "Modeling Directional Two Arm Archimedes Spiral Coils in the RF Electromagnet Range", COMSOL Conference, Boston, 2008.

9. Acknowledgements

This work was sponsored by the Naval Undersea Warfare Center's In-house Laboratory Independent Research Program. The author would also acknowledge the RF model set up help received from COMSOL staff member Bjorn and to NUWC's Jason Maguire for discussions on the elliptical coils.